Flexible and Printed Electronics



# Highly sensitive and fully printable humidity sensor on a flexible substrate based on a zinc oxide and polyethylenimine composite

To cite this article: Fatemeh Samaeifar *et al* 2022 *Flex. Print. Electron.* **7** 034003

IOP Publishing Flex. Print. Electron. 7 (2022) 034003 https://doi.org/10.1088/2058-8585/ac8f58

Flexible and Printed Electronics



OPEN ACCESS

RECEIVED
21 July 2022

REVISED
17 August 2022

ACCEPTED FOR PUBLICATION
5 September 2022

PUBLISHED
19 September 2022



PAPER

# Highly sensitive and fully printable humidity sensor on a flexible substrate based on a zinc oxide and polyethylenimine composite

**Fatemeh Samaeifar[1,*], Mohsen Azadinia[1], Atefeh Ghorbani[1], Junfei Chen[1], Mathieu Gratuze[2], Mohsen Ketabi[2], Ricardo Izquierdo[2] and Hany Aziz[1]**

[1] Department of Electrical and Computer Engineering and Waterloo Institute for Nanotechnology, University of Waterloo, 200 University Avenue West, Waterloo, Ontario N2L 3G1, Canada
[2] Department of Electrical Engineering, École de Technologie Supérieure (ETS), 1100 Notre-Dame St W, Montreal, QC H3C 1K3, Canada
[*] Author to whom any correspondence should be addressed.

**E-mail:** fsamaeif@uwaterloo.ca

**Keywords:** flexible electronics, green printed electronics, humidity sensors, metal oxide, capacitive sensors

Supplementary material for this article is available online

## Abstract

We report a highly sensitive and fully printable capacitive humidity sensor based on a zinc oxide (ZnO) and polyethylenimine (PEI) composite. The sensor has a simple structure, consisting only of a layer of the ZnO:PEI composite, coated using an ethanol solution, on a layer of silver inter-digital electrodes that have been pre-printed on a polyethyleneterephthalate substrate. The sensor with ZnO:PEI in the ratio of 2:1 by volume exhibits a response of 43 907 000% at maximum humidity, with a detection range of 15%–95% relative humidity, higher than other sensors fully made by wet-coating processes. Fourier transform infrared spectroscopy, atomic force microscopy, and scanning electron microscopy measurements suggest that the high response likely arises from the use of a hydrophilic polymer with a high dipole moment which facilitates dipole-dipole interactions with water molecules and from the highly granular morphology of the composite which leads to a high surface-to-volume ratio and more-numerous water adsorption sites. The fabricated sensor also demonstrates short response/recovery times (5 s/3 s), good repeatability over multiple humidification and desiccation cycles, and only 5% loss in response after being kept in the ambient for three weeks.

## 1. Introduction

Humidity sensors detect the water content through a change in various parameters including resistance, capacitance, surface acoustic waves, and piezoelectric. Among these, the first two attract a special interest because of their easy integration into electronic circuits [1]. In comparison to resistive sensors, capacitive ones tend to have a faster response and higher stability. They also offer easier integration with smart systems where communication between the sensor and an electronic device needs to be done wirelessly and remotely [2, 3].

In recent years, with the growing use of ubiquitous electronics and internet of things systems, there is an increasing demand for using humidity sensors as standalone devices or as components in smart monitoring systems for a variety of applications [4–11]. One such application is in the emerging 'smart packaging' industry for products that can be sensitive to moisture, such as food, pharmaceuticals, and cosmetics. Integrating a humidity sensor in the packaging material would allow recording or monitoring humidity levels during storage or transportation, helping to ensure product quality.

To be suitable for smart packaging applications, a humidity sensor must not only have adequate sensitivity and stability, but also be possible to fabricate on various surfaces or substrates [12, 13]. Meeting these requirements while also keeping manufacturing cost low enough to be feasible for packaging and disposable electronics is often challenging [14]. The requirement to use of green materials also adds additional constraints [15, 16]. Conventionally, humidity sensors have been manufactured on rigid structures like glass or ceramics, using techniques such

as photolithography and sputtering [17–19]. These techniques are relatively expensive, time consuming, and require high vacuum processes, and therefore do not satisfy the cost constraints of the packaging industry. Moreover, the rigid nature of the substrates prevents their use in applications which require mechanical flexibility and conformal form factors. Thus, extensive efforts have been devoted to the development of humidity sensors on flexible, non-conventional substrates in recent years, such as polyethylene terephthalate (PET), polyimide (PI), cellulose paper, etc [16, 20–22]. However, challenges still exist for the realization of reliable humidity sensors manufactured by low cost printing processes, using eco-friendly solvents on flexible substrate [23].

Recently, the use of metal oxides such as $SnO_2$, $TiO_2$, $WO_3$, ZnO, $Al_2O_3$, and $Fe_3O_4$ in humidity sensors has received significant attention due to their low cost and ease of fabrication. These materials typically have granular morphologies and textures that allow for increased adsorption of water molecules [23–25]. ZnO is perhaps the most widely employed and researched material, owing to a combination of favorable characteristics such as a wide band gap of 3.37 eV, high chemical and thermal stability, and high mechanical strength [26–28]. However, ZnO-based humidity sensors suffer some limitations, such as low sensitivity especially at low humidity levels and large hysteresis. To overcome some of these shortcomings, ZnO is sometimes combined with other semiconducting materials [29–31] or polymers [32, 33]. Polyethyleneimine (PEI) is a hydrophilic polymer that is commonly used to fabricate hydrogels [34]. It has also been previously utilized as a sensing layer in quartz crystal microbalance-based formaldehyde humidity sensors [35] because of its high dipole moment [35], which helps increase adsorption and interactions with water molecules through dipole-dipole interactions.

In this work we report a novel humidity sensor based on combining ZnO with PEI. ZnO and PEI have a relative dielectric permittivity of ∼5–6 [36] and ∼9, respectively [37], we, therefore, expected a composite of ZnO and PEI (ZnO:PEI) to be suitable for a capacitive-type sensor, and to exhibit significant changes in dielectric constant when exposed to moisture. To test this hypothesis, we coated a ZnO:PEI composite layers on flexible PET substrates, pre-printed with silver inter-digital electrodes (IDEs), by spin coating using ethanol as a solvent. The ZnO:PEI (2:1 volume ratio) sensor exhibits a response of 43 907 000%, higher than other sensors fully made by wet-coating processes, with a detection range of 15%–95% relative humidity (RH), as well as fast response and recovery times of 5 s and 3 s, respectively.

## 2. Experimental details

### 2.1. Material preparation and device fabrication

ZnO and PEI were purchased from Sigma-Aldrich (USA). ZnO sol–gel was prepared by dissolving 197 mg zinc acetate in 6 ml ethanol (Sigma-Aldrich) plus 54 $\mu$l ethanolamine (Sigma-Aldrich), and mixing at 700 rpm for 50 min at 45 °C. The PEI solution was prepared by stirring 33 mg branched-PEI in 1 ml ethanol (Sigma-Aldrich) at 700 rpm overnight. The ZnO solution was then mixed with the PEI solution in the ratio of 2 to 1 (i.e. around 66.66%:33.34%), or 1 to 1 (i.e. around 50%:50%), by volume, stirring at 700 rpm for 1 h. All solutions were filtered through a 0.22 $\mu$m polypropylene filter before spin-coating. Energy dispersive x-ray measurements of ZnO:PEI (2:1 volume ratio) were conducted to determine the elemental composition of composite film, as shown in figure S1. The weight percentage of C, O, Zn, and N in the composite is 39.46%, 31.92%, 19.07% and 8.31%, respectively.

20 mm × 20 mm PET substrates with silver IDEs, with 250 $\mu$m finger width and 200 $\mu$m gap, were provided by Printability and Graphic Communications Institute (ICI). The substrates with the IDEs were cleaned by sonicating in isopropanol, and temporarily attached to a piece of glass to facilitate mounting on a spin-coater. ZnO, PEI, ZnO:PEI (2:1 volume ratio), or ZnO:PEI (1:1 volume ratio) solutions were then spin-coated on the IDEs at 1000 rpm for 1 min and pre-annealed at 150 °C for 30 min, followed by annealing at 120 °C for a period of 8–12 h in the oven. Figures 1(a)–(c) show the molecular structure of PEI, an optical top view image of the substrate with the IDEs, and a schematic 3D illustration of the fabricated sensors, respectively. Figure 1(d) also shows an optical image of a fully fabricated sensor with ZnO:PEI (2:1 volume ratio) under bending, demonstrating the flexibility of the fabricated sensors.

### 2.2. Measurement setup

The measurement were conducted in an airtight homemade box using a KEYSIGHT Digital U1733C hand-held LCR meter for measuring capacitance. The box was connected to a humidity generator using nitrogen as a carrier gas with adjustable dry/wet gas ratios to achieve the desired RH levels. A commercial SHT40 sensor with a resolution of 0.01% RH, accuracy of ±1.8% RH, and time response of <4 s was used as a reference sensor. For data acquisition, a personal computer was used, while the fabricated sensor data was analyzed using the software built into the KEYSIGHT Digital U1733C hand-held LCR meter. Figure 1(e) shows a schematic diagram of the experimental setup.

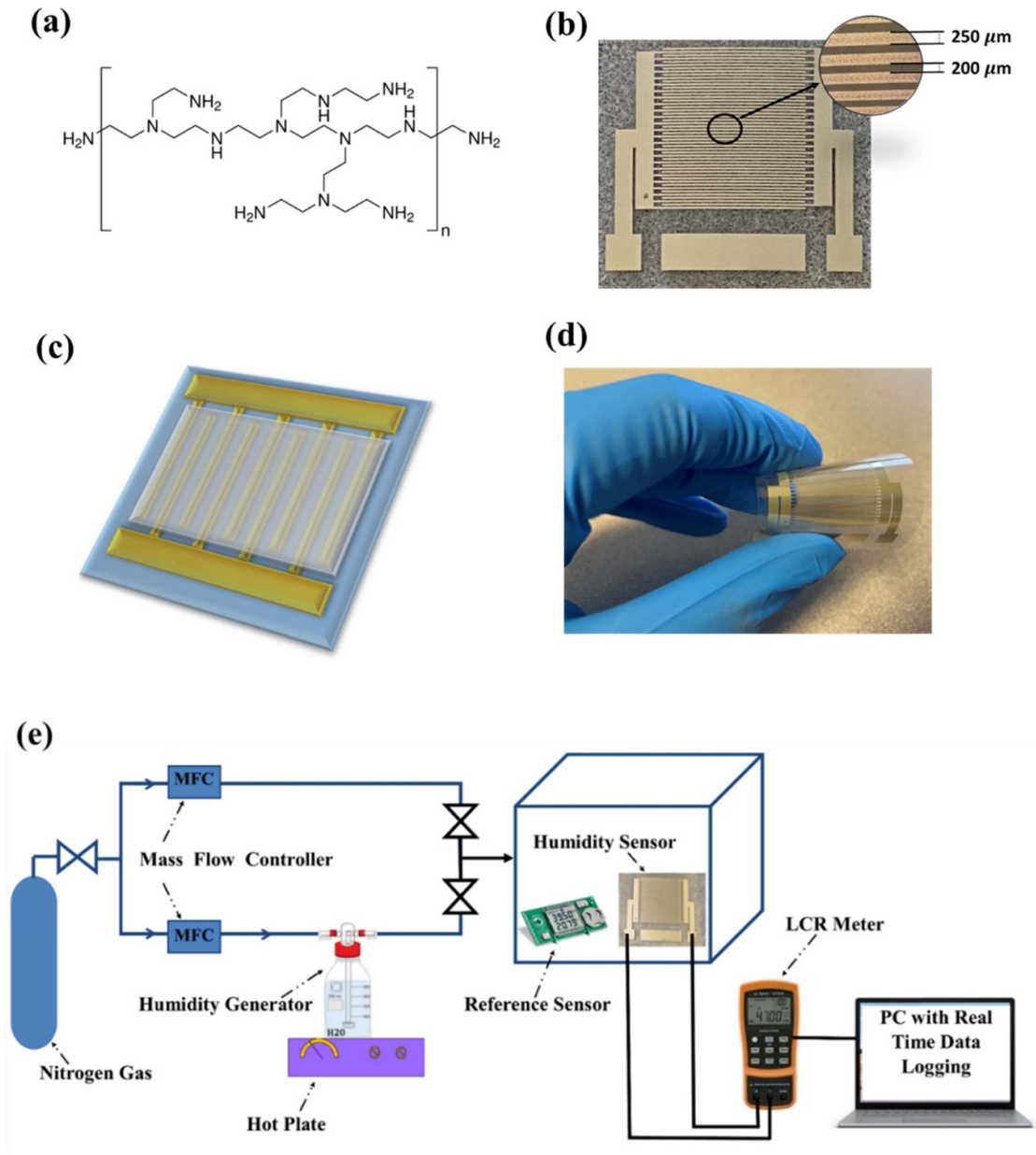


**Figure 1.** (a) Molecular structure of PEI. (b) An optical top view image of the substrate with the IDEs. (c) Schematic 3D illustration of the fabricated sensor. (d) An image of the fully fabricated sensor under bending. (e) A schematic diagram of the experimental setup.

## 3. Results and discussion

The sensors with ZnO, PEI, ZnO:PEI (1:1 volume ratio), and ZnO:PEI (2:1 volume ratio) layers, the latter two denoted to later by ZnO:PEI (1:1) and ZnO:PEI (2:1), respectively, were placed in the test box, and the RH was increased from 10% to 90%. Figures 2(a) and (b) show changes in capacitance of these sensors as function of changes in RH levels measured at room temperature at 1 kHz and 100 Hz, respectively. The presented data represents the average values from measurements on 10 different samples in each case. The error bars represent the typical variation in the measured data among the devices. To help visualize the changes in capacitance at low RH levels, a logarithmic scale is used for the *y*-axis, with the insets presenting the same data using non-logarithmic scales for RH > 50%.

The capacitance increased monotonically with RH for all sensors, exhibiting a somewhat linear trend over the 50%–95% RH range as can be seen in the insets. The increase is however much larger in case of the ZnO:PEI sensors, amounting to almost five orders of magnitude. Also remarkably, the onset for capacitance increase occurs at a much lower RH value in case of the ZnO:PEI sensors, starting at 15% RH versus 40%–45% RH in case of their ZnO and PEI

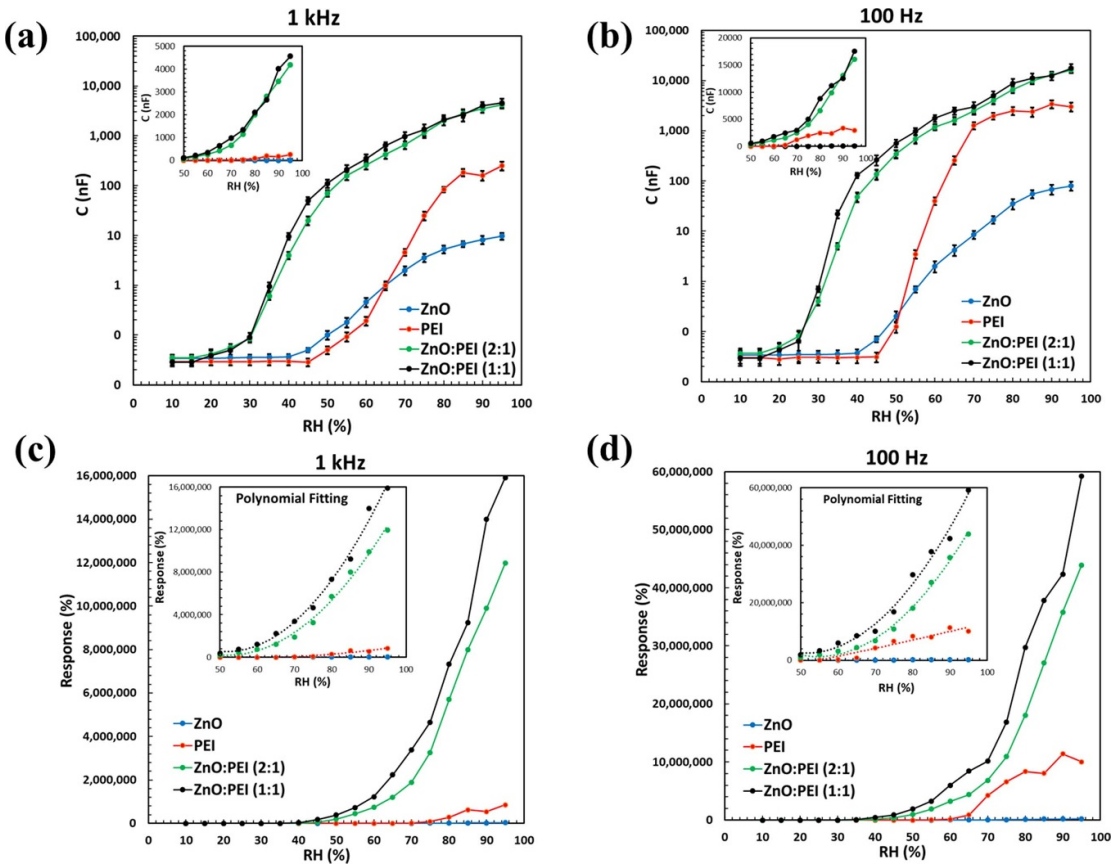


**Figure 2.** Capacitance vs RH of the ZnO, PEI, ZnO:PEI (2:1), and ZnO:PEI (1:1) measured at room temperature at (a) 1 kHz, and (b) 100 Hz. The insets present the same data using non-logarithmic scales for RH > 50%. Calculated response vs RH of the same sensors at (c) 1 kHz, and (d) 100 Hz. The insets show polynomial fits of the same data over the 50%–95% range.

counterparts, indicating that the composite gives a wider detection range.

In a capacitance humidity sensor, response and average sensitivity, $S$, of are defined by [38–41]:

$$\text{Response} = \frac{C_{RH} - C_{RH(min)}}{C_{RH(min)}} \times 100 \qquad (1)$$

$$S = \frac{C_{RH(max)} - C_{RH(min)}}{RH_{max} - RH_{min}} \qquad (2)$$

where $C_{RH}$ is the capacitance of the sensor at any given RH, and $C_{RH(max)}$ and $C_{RH(min)}$ correspond to the measured capacitance at the highest and lowest recorded RH levels, respectively. Figures 2(c) and (d) present response versus RH curves at 1 kHz and 100 Hz of the sensors, respectively, using the capacitance values in figures 2(a) and (b), and equation (1). The insets in figures 2(c) and (d) give polynomial fits of the same data in the humidity range of 50%–95% RH. The sensors with ZnO, PEI, ZnO:PEI (2:1) PEI, and ZnO:PEI (1:1) layers show the respective response of 28 743%, 849 662%, 11 976 220%, and 15 907 217% at l kHz, and of 234 840%, 10 033 345%, 43 907 000%, and 59 195 846% at 100 Hz.

According to equation (2), the sensitivity of the humidity sensor is expressed as a change of the measured signal per RH unit (i.e. the slope of the calibrated linear fitting response line). Generally, the humidity sensor has poor linear characteristics in a wide RH range [38], hence, mostly the slope of the polynomial fitting response line is considered as the sensor sensitivity [39, 40, 42]. The sensors with ZnO, PEI, ZnO:PEI (2:1) PEI, and ZnO:PEI (1:1) layers show the respective sensitivities of 213 pF/%RH, 5550 pF/%RH, 92 000 pF/%RH, and 99 000 pF/%RH at l kHz, and of 1772 pF/%RH, 67 000 pF/%RH, 350 000 pF/%RH, and 370 000 pF/%RH at 100 Hz in the humidity range of 50%–95% RH. The results are summarized in table 1.

All sensors show larger capacitance changes at 100 Hz compared with 1 kHz, which is expected as the relative permittivity of the capacitor decreases with increasing frequency [43], and is consistent with previous reports [43, 44]. As seen, the response of the ZnO:PEI sensors is about 200–250 times higher at 100 Hz and 400–550 times higher at 1 kHz than that of ZnO sensor. It is also about 4–6 times higher at 100 Hz and 14–19 times higher at 1 kHz than that of PEI sensor. Decreasing the ZnO ratio in the ZnO:PEI composite (i.e. from 2:1 to 1:1, by volume)

**Table 1.** RH range, response and sensitivity of fabricated sensors.

| Sensor | Detection range | Sensitivity (50%–95% RH) (pF/%RH) | | Response (95% RH)(%) | |
|---|---|---|---|---|---|
| | | 1 kHZ | 100 Hz | 1 kHz | 100 Hz |
| ZnO | 40%–95% | 213 | 1772 | 28 743 | 234 840 |
| PEI | 45%–80% | 5550 | 67 000 | 849 662 | 10 033 345 |
| ZnO:PEI (2:1) | 15%–95% | 92 000 | 350 000 | 11 976 220 | 43 907 000 |
| ZnO:PEI (1:1) | 15%–95% | 99 000 | 370 000 | 15 907 217 | 59 195 846 |

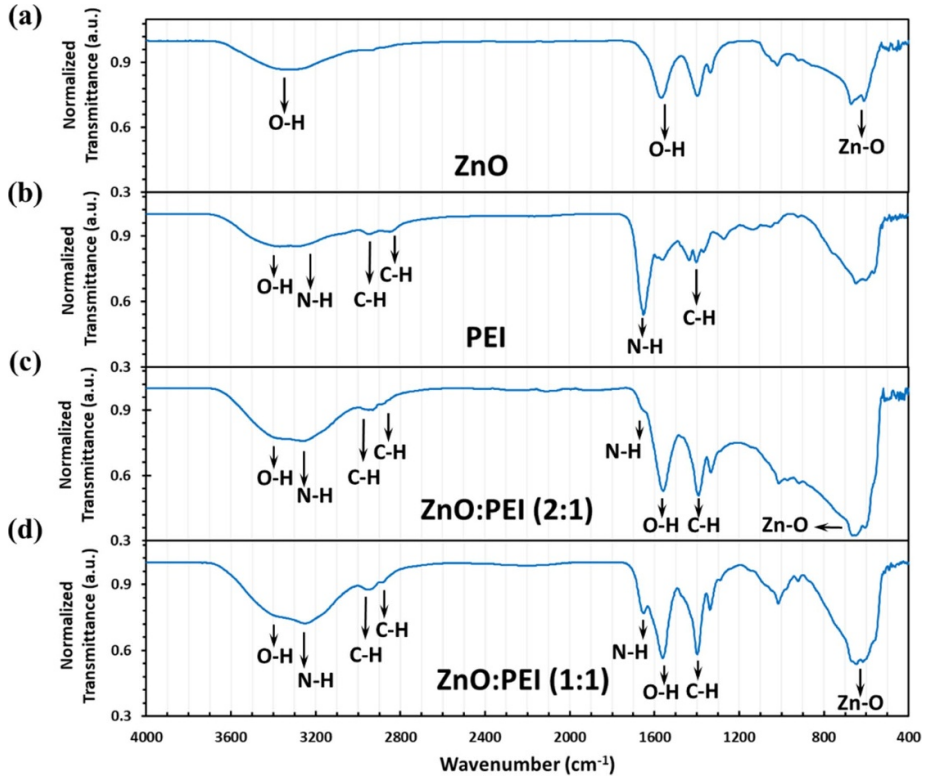


**Figure 3.** FTIR spectra of moisture-exposed (a) ZnO, (b) PEI, (c) ZnO:PEI (2:1), and (d) ZnO:PEI (1:1) films.

leads to a slight improvement in sensor response; however, the former exhibits a more linear response, as seen in the insets of figures 2(a) and (b). Thus, the higher ratio, i.e. ZnO:PEI (2:1), is considered to be more optimum. Also, notably, the response of the PEI sensor is higher than that of the ZnO sensor, which may be ascribed to its higher polarity (reflected in its higher relative permittivity) that would increase dipole-dipole interactions with $H_2O$ molecules, and hence more adsorption. PEI also notably loses its linearity at RH > 80%, displaying some saturation effect. Although the underlying causes for this behavior are still unknown, it may suggest that the PEI film surface becomes more easily saturated with adsorbed $H_2O$ molecules, possibly due to morphological factors (e.g. smoother topography).

To glean some insights into the factors underlying the higher response of the ZnO:PEI sensors, the chemical bonding structures of moisture-exposed ZnO, PEI, and their composite films were investigated by Fourier transform infrared spectroscopy (FTIR). The results are shown in figure 3. The 520 $cm^{-1}$ band in the spectrum of ZnO (in figure 3(a)) can be ascribed to Zn–O bond stretching [33], whereas the broad bands at 3334 $cm^{-1}$ and at 1330 $cm^{-1}$–1670 $cm^{-1}$ can be ascribed to O–H bond stretching and bending, respectively, and point to the presence of moisture in the films [45, 46]. Figure 3(b), showing the spectrum of PEI, displays vibrational bands located at 3400 $cm^{-1}$, 3272 $cm^{-1}$, 2940 $cm^{-1}$ and 2815 $cm^{-1}$, 1676 $cm^{-1}$, and 1465 $cm^{-1}$ corresponding to O–H stretching, N–H stretching, C–H stretching, C–H stretching, N–H bending, and C–H bending, respectively [47]. The spectra of the ZnO:PEI composites, shown in figures 3(c) and (d), demonstrating the same bands as in the ZnO and PEI films, and no new bands, indicating that no chemical reactions occur between ZnO and PEI in the composites. Interestingly, the intensity of the 3434 $cm^{-1}$ band, associated with hydroxyl residue,

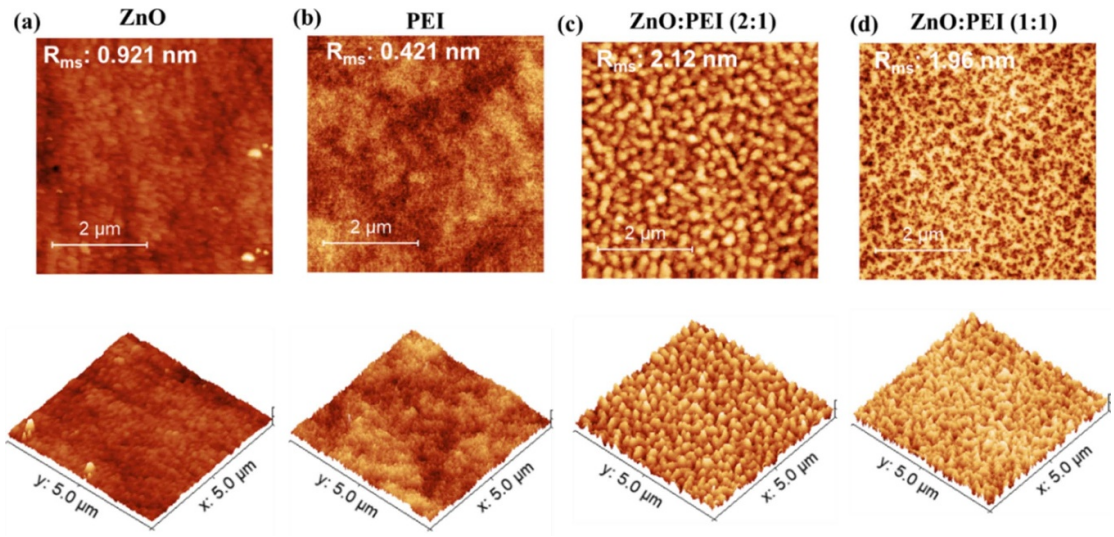


**Figure 4.** AFM images of (a) ZnO, (b) PEI, (c) ZnO:PEI (2:1), and (d) ZnO:PEI (1:1) films.

increases in the composites. Moreover, the intensity of the N–H bond stretching increases and shifts to higher wavenumbers in the composites, evidence of more water content compared with the neat materials [33, 48]. While, from the FTIR results, we can attribute the higher response of the neat PEI sensor relative to its ZnO counterpart to the higher affinity of PEI to moisture, which may be ascribed to its more polar nature as suggested earlier, additional factors must be contributing to the much higher response of the composite sensors and their much greater capacity for adsorbing water relative to the neat PEI.

We therefore also study the surface morphology of the thin films of ZnO, PEI, and their composites using atomic force microscopy (AFM). The results are shown in figure 4. As can be seen from the images, unlike the neat films, the composites exhibit a granular morphology. The surface roughness (Rms) of the ZnO, PEI, ZnO:PEI (2:1), and ZnO:PEI (1:1) films are 0.921 nm, 0.421 nm, 2.12 nm, and 1.96 nm, respectively. The surface morphology of the ZnO and ZnO:PEI (2:1) was also characterized by field-emission scanning electron microscopy, as shown in figures S2(a) and (b). The SEM images again show that the composite film has a more granular morphology, pointing toward a high surface area to volume ratio for maximum adsorption of the water molecules compared with neat film. From the higher surface roughness and granular morphology one can expect the composite films to have much more surface area for water adsorption than the ZnO and PEI films. It is therefore possible that the granular morphology and greater surface roughness of the composite films is behind their much higher moisture adsorption capacity, in turn leading to higher sensor response.

Based on the above results, we may ascribe the improved humidity sensing performance of these sensors to increased water absorption on the ZnO:PEI surface. At low RH values, $OH^-$ and $H^+$, from $H_2O$ dissociation [30], are chemisorbed on the ZnO:PEI layer surface. At high RH values, physisorption will occur on the chemisorbed water layer and creates a layer of water molecules weakly bonded by Van der Waals interactions [49]. As the humidity level increases further, the new layers of physisorbed water molecules are formed on top of the previous one. This will increase the dipole moment of the ZnO:PEI layer, further increasing its capacitance [24]. Figure S3 illustrates the general humidity sensing mechanism.

The stability, hysteresis, repeatability, response time, and recovery time of the ZnO:PEI (2:1) sensor were also investigated. For the stability test, the capacitance vs RH characteristics were measured after 1, 2, and 3 weeks of keeping the sensor in ambient conditions without encapsulation. Figures 5(a) and (b) show the results of the stability tests recorded at 1 kHz and 100 Hz, respectively, with the insets again showing the same data using non-logarithmic scales on a $y$-axis for RH > 50%. As can be seen from the figures, the characteristics hardly change over the three weeks period. The response of the ZnO:PEI (2:1) sensor decreased by only 5%, changing from 11 976 220% to 11 412 200% after 3 weeks of being kept in the ambient when measured at 1 kHz, and by only 7%, decreasing from 43 907 000% to 40 983 400%, when measured at 100 Hz. These results indicate that the fabricated sensor has a very high ambient stability.

Humidity hysteresis, defined as the maximum difference of measured signal during the process of adsorption and desorption of water molecules, is also an important consideration in a sensor [38]. Such differences may arise form charge trapping in the sensor layers or differences in water adsorption and desorption rates [39, 50]. Figure 6(a) shows the

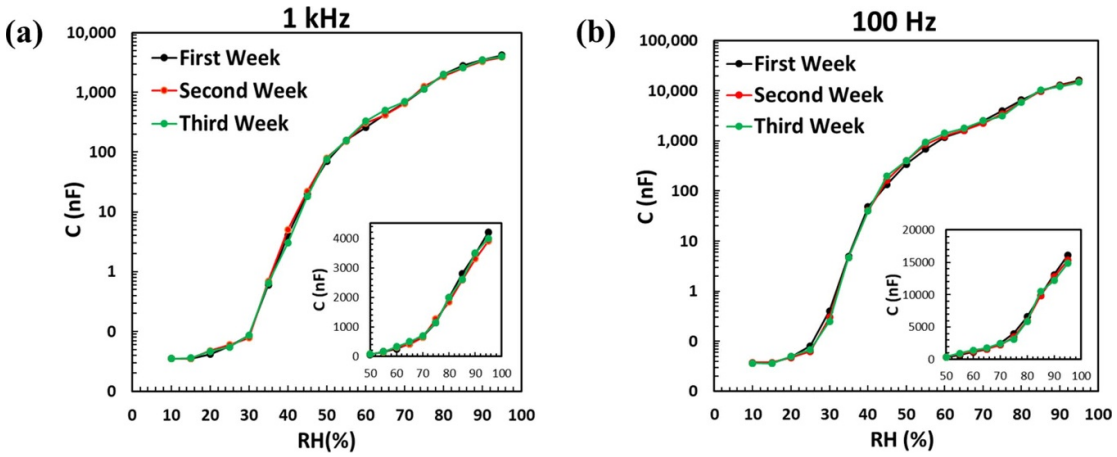


**Figure 5.** Capacitance versus humidity response characteristics of the ZnO:PEI (2:1) sensor measured over the RH range from 10% to 95% at (a) 1 kHz, and (b) 100 Hz after 1, 2 and 3 weeks of the sensor being kept in ambient conditions without encapsulation.

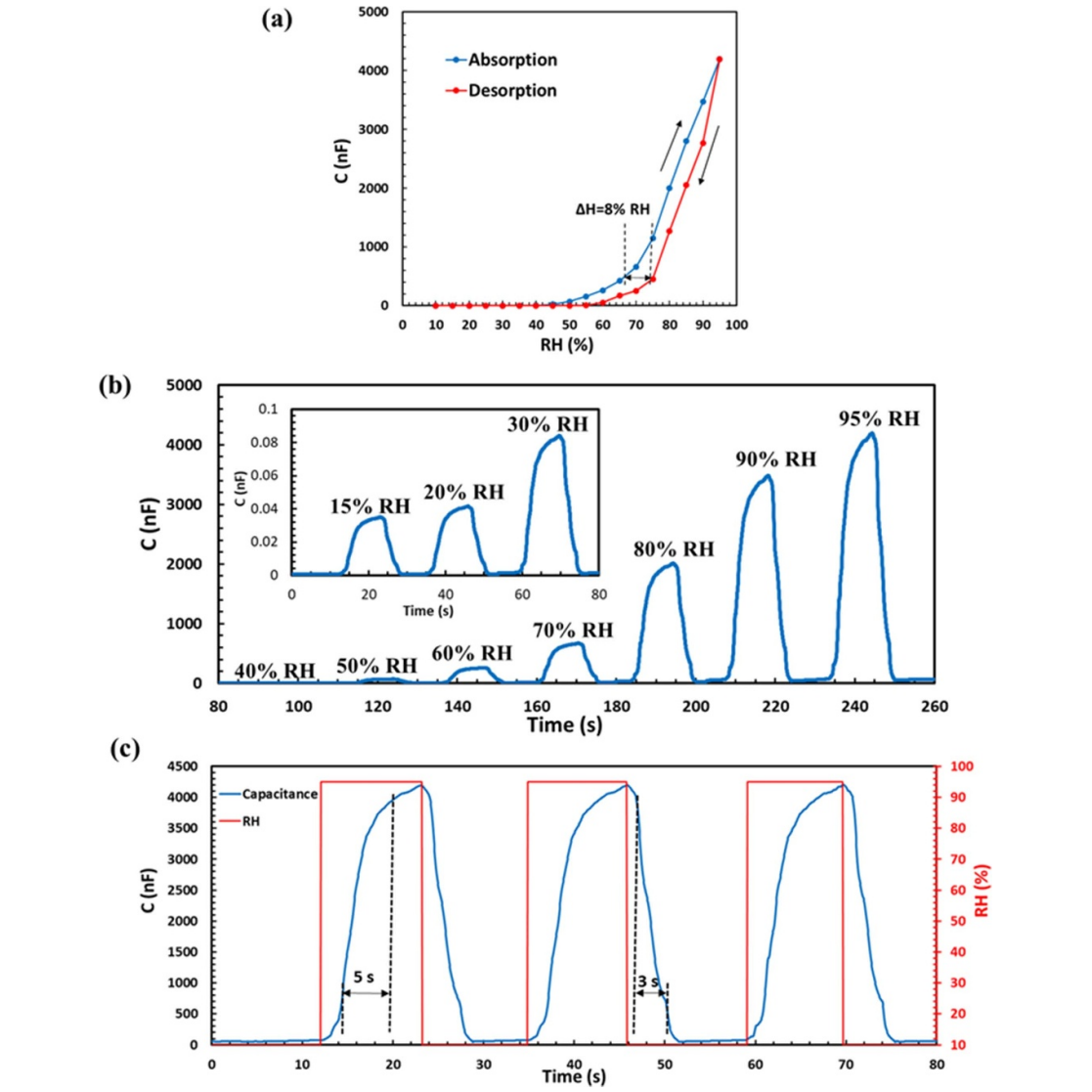


**Figure 6.** (a) Capacitance versus RH measured on increasing the RH from 10% to 95% (blue) and on decreasing the RH from 95% to 10% (red) to test differences in response in adsorption versus desorption. (b) Dynamic response curve to the increasing RH from 40% to 95%, and the inset is the amplified dynamic response curve within 15%–30% RH. (c) Repeatability performance of the sensor exposed to 95% RH from 10% RH. All measurements were done for ZnO:PEI (2:1) sensor at 1 kHz.

**Table 2.** Comparison of humidity-sensing performance between the printable ZnO:PEI (2:1) humidity sensor and other reported printable sensors.

| Sensor Type | Frequency | Detection range | Response Time | Recovery Time | Response (at max humidity) | References |
|---|---|---|---|---|---|---|
| Capacitance | 1 kHz | 0%–85% | 1 s | 2 s | 13% | [1] |
| Impedance | — | 0%–80% | 1 s | 10.75 s | 700% | [52] |
| Capacitance | 1 kHz | 0%–90% | 1.99 s | 8.76 s | 108% | [53] |
| Capacitance | 1 kHz | 20%–90% | 0.96 s | 1.03 s | 1100% | [39] |
| Resistance | — | 5%–98% | 30 s | 51 s | 341 700% | [33] |
| Capacitance | 100 Hz | 12%–95% | 12 s | 3 s | 4900% | [54] |
| Resistance | — | 20%–80% | 20 s | 35 s | 300% | [55] |
| Capacitance | 100 kHz | 20%–90% | 250 s | 175 s | 350% | [56] |
| Capacitance | 100 Hz | 5%–95% | 21.4 s | 4.8 s | 100% | [43] |
| Capacitance | 100 Hz | 11%–97% | 4.7 s | 3 s | 4450 544% | [57] |
| Capacitance | 1 kHz | 5%–95% | — | — | 2 869 500% | [58] |
| Capacitance | 100 Hz | 15%–95% | 5 s | 3 s | 43 907 000% | This work |
| Capacitance | 1 kHz | 15%–95% | 5 s | 3 s | 11 976 220% | This work |

capacitance vs RH characteristics of the ZnO:PEI (2:1) sensor measured under humidification (RH increasing from 10% to 95%) and desiccation (RH decreasing from 95% to 10%). The humidity hysteresis of the sensor is about 8% and occurred at around 75% RH which is somewhat high but comparable to other sensors made by wet-coating.

Figure 6(b) shows the dynamic response curve to the increasing RH from 40% to 95%, and the inset is the amplified dynamic response curve within 15%–30% RH, which clearly shows that the humidity sensor has good response to low RH range (15%). Figure 6(c) presents repeatability performance of the ZnO:PEI (2:1), exposed to 95% RH from 10% RH. This result shows that he sensor displays good repeatability, evident from the consistent response characteristics over three cycles.

We also calculated the response and recovery times of the sensor, as shown in figure 6(c). The response and recovery times are defined as the time needed for the capacitance of the sensor vary from 10% to 90% of its final value during the humidification and the desiccation processes, respectively [31, 51]. As seen, the sensor response and recovery times are 5 s and 3 s, respectively, on par with the fastest speeds observed from other printable capacitive humidity sensors.

Table 2 compares the performance parameters of the ZnO:PEI (2:1) sensor of this work with those of other printable humidity sensors previously reported. The composite sensor demonstrates a significantly higher response in comparison to other sensors, along with a competitive set of other parameters including RH range, response and recovery times and high ambient stability. Based on these results, coupled with its simple structure, ease of fabrication and its use of only eco-friendly materials, we believe that the ZnO:PEI humidity sensor has a significant potential for smart packaging and other humidity sensing applications.

## 4. Conclusion

In summary, a highly-sensitive and fully printable capacitive humidity sensor based on ZnO and PEI composite has been reported. The sensor has a simple structure, consisting only of a layer of the ZnO:PEI composite, coated atop IDEs pre-printed on a PET substrate, using alcohol solvent. The ZnO:PEI (2:1) sensor showed a response of 43 907 000% at 100 Hz, which is higher than other sensors fully made by wet-coating processes, with detection range of 15%–95% RH at room temperature. The sensor also has fast response and recovery times (5 s and 3 s, respectively) and exhibited good repeatability over multiple humidification and desiccation cycles. Long-term stability tests indicate that the sensor possesses high stability under ambient conditions, with response differences of below 5% at 1 kHz and 7% at 100 Hz, after three weeks of being kept in the ambient without encapsulation. This work demonstrates that ZnO:PEI sensor is a promising candidate for smart packaging and other humidity sensing applications.

## Data availability statement

All data that support the findings of this study are included within the article (and any supplementary files).

## ORCID iD

Fatemeh Samaeifar https://orcid.org/0000-0002-4789-588X

## References


[1] Hassan G, Bae J, Lee C H and Hassan A 2018 Wide range and stable ink-jet printed humidity sensor based on graphene and zinc oxide nanocomposite *J. Mater. Sci., Mater. Electron.* **29** 5806–13

[2] Duan Z, Zhao Q, Wang S, Yuan Z, Zhang Y, Li X, Wu Y, Jiang Y and Tai H 2020 Novel application of attapulgite on high performance and low-cost humidity sensors *Sens. Actuators* B **305** 127534

[3] Najeeb M A, Ahmad Z and Shakoor R A 2018 Organic thin-film capacitive and resistive humidity sensors: a focus review *Adv. Mater. Interfaces* **5** 1800969

[4] Jiang B, Bi Z, Hao Z, Yuan Q, Feng D, Zhou K, Zhang L, Gan X and Zhao J 2019 Graphene oxide-deposited tilted fiber grating for ultrafast humidity sensing and human breath monitoring *Sens. Actuators* B **293** 336–41

[5] Cao Q, Yu C, Cheng X-F, Sun W-J, He J-H, Li N-J, Li H, Chen D-Y, Xu Q-F and Lu J-M 2020 Polysquaramides: rapid and stable humidity sensing for breath monitoring and morse code communication *Sens. Actuators* B **320** 128390

[6] Li X, Zhuang Z, Qi D and Zhao C 2021 High sensitive and fast response humidity sensor based on polymer composite nanofibers for breath monitoring and non-contact sensing *Sens. Actuators* B **330** 129239

[7] Shrivastav A M, Gunawardena D S, Liu Z and Tam H-Y 2020 Microstructured optical fiber based Fabry–Pérot interferometer as a humidity sensor utilizing chitosan polymeric matrix for breath monitoring *Sci. Rep.* **10** 1–10

[8] Samaeifar F, Ceccacci A C, Goswami S B, Nielsen L H, Afifi A, Zór K and Boisen A 2019 Evaluation of the solid state form of tadalafil in sub-micron thin films using nanomechanical infrared spectroscopy *Int. J. Pharm.* **565** 227–32

[9] Zhao Q, Duan Z, Wu Y, Liu B, Yuan Z, Jiang Y and Tai H 2022 Facile primary battery-based humidity sensor for multifunctional application *Sens. Actuators* B **370** 132369

[10] Zhang Y, Wu Y, Duan Z, Liu B, Zhao Q, Yuan Z, Li S, Liang J, Jiang Y and Tai H 2022 High performance humidity sensor based on 3D mesoporous $Co_3O_4$ hollow polyhedron for multifunctional applications *Appl. Surf. Sci.* **585** 152698

[11] Zhao Q *et al* 2022 A $Nb_2CT_x$/sodium alginate-based composite film with neuron-like network for self-powered humidity sensing *Chem. Eng. J.* **438** 135588

[12] Park K-J and Gong M-S 2017 A water durable resistive humidity sensor based on rigid sulfonated polybenzimidazole and their properties *Sens. Actuators* B **246** 53–60

[13] Eryürek M, Tasdemir Z, Karadag Y, Anand S, Kilinc N, Alaca B E and Kiraz A 2017 Integrated humidity sensor based on SU-8 polymer microdisk microresonator *Sens. Actuators* B **242** 1115–20

[14] Duan Z, Zhao Q, Wang S, Huang Q, Yuan Z, Zhang Y, Jiang Y and Tai H 2020 Halloysite nanotubes: natural, environmental-friendly and low-cost nanomaterials for high-performance humidity sensor *Sens. Actuators* B **317** 128204

[15] Zhuang Z, Li Y, Qi D, Zhao C and Na H 2017 Novel polymeric humidity sensors based on sulfonated poly (ether ether ketone) s: influence of sulfonation degree on sensing properties *Sens. Actuators* B **242** 801–9

[16] Duan Z, Jiang Y, Yan M, Wang S, Yuan Z, Zhao Q, Sun P, Xie G, Du X and Tai H 2019 Facile, flexible, cost-saving, and environment-friendly paper-based humidity sensor for multifunctional applications *ACS Appl. Mater. Interfaces* **11** 21840–9

[17] Oprea A, Courbat J, Bârsan N, Briand D, De Rooij N and Weimar U 2009 Temperature, humidity and gas sensors integrated on plastic foil for low power applications *Sens. Actuators* B **140** 227–32

[18] Kannan P K, Saraswathi R and Rayappan J B B 2010 A highly sensitive humidity sensor based on DC reactive magnetron sputtered zinc oxide thin film *Sens. Actuators* A **164** 8–14

[19] Abdollahi H, Samaeifar F, Afifi A and Aliahmadi M 2017 External alignment marks technique for front-to-back side alignment using single-side mask aligner *Exp. Tech.* **41** 627–34

[20] Duan Z, Yuan Z, Jiang Y, Zhao Q, Huang Q, Zhang Y, Liu B and Tai H 2022 Power generation humidity sensor based on primary battery structure *Chem. Eng. J.* **446** 136910

[21] Duan Z, Jiang Y, Huang Q, Wang S, Wang Y, Pan H, Zhao Q, Xie G, Du X and Tai H 2021 Paper and carbon ink enabled low-cost, eco-friendly, flexible, multifunctional pressure and humidity sensors *Smart Mater. Struct.* **30** 055012

[22] Tai H, Duan Z, Wang Y, Wang S and Jiang Y 2020 Paper-based sensors for gas, humidity, and strain detections: a review *ACS Appl. Mater. Interfaces* **12** 31037–53

[23] Hassan G, Bae J and Lee C H 2018 Ink-jet printed transparent and flexible electrodes based on silver nanoparticles *J. Mater. Sci., Mater. Electron.* **29** 49–55

[24] Shakya V, Pandey N, Misra S K and Roy A 2017 Electrical and optical properties of ZnO–$WO_3$ nanocomposite and its application as a solid-state humidity sensor *Bull. Mater. Sci.* **40** 253–62

[25] Hossein-Babaei F, Moghadam S and Masoumi S 2015 Forming ohmic Ag/$SnO_2$ contacts *Mater. Lett.* **141** 141–4

[26] Abutalib M and Rajeh A 2020 Structural, thermal, optical and conductivity studies of Co/ZnO nanoparticles doped CMC polymer for solid state battery applications *Polym. Test.* **91** 106803

[27] Zhang H, Zhang M, Lin C and Zhang J 2018 AuNPs hybrid black ZnO nanorods made by a sol-gel method for highly sensitive humidity sensing *Sensors* **18** 218

[28] Azadinia M, Fathollahi M, Mosadegh M, Boroumand F and Mohajerani E 2017 Improved performance of photoconductive gain hybrid UV detector by trap state engineering of ZnO nanoparticles *J. Appl. Phys.* **122** 154501

[29] Feng M H and Li X J 2018 Capacitive humidity-sensing properties of ZnO nanorods/silicon nanoporous pillar array enhanced by LiCl incorporation *Sens. Actuators* B **272** 543–9

[30] Burman D, Choudhary D S and Guha P K 2019 ZnO/$MoS_2$-based enhanced humidity sensor prototype with Android app interface for mobile platform *IEEE Sens. J.* **19** 3993–9

[31] Li B, Tian Q, Su H, Wang X, Wang T and Zhang D 2019 High sensitivity portable capacitive humidity sensor based on $In_2O_3$ nanocubes-decorated GO nanosheets and its wearable application in respiration detection *Sens. Actuators* B **299** 126973

[32] Deka B J, Guo J, Khanzada N K and An A K 2019 Omniphobic re-entrant PVDF membrane with ZnO nanoparticles composite for desalination of low surface tension oily seawater *Water Res.* **165** 114982

[33] Arularasu M, Harb M, Vignesh R, Rajendran T and Sundaram R 2020 PVDF/ZnO hybrid nanocomposite applied as a resistive humidity sensor *Surf. Interfaces* **21** 100780

[34] Tai H, Bao X, He Y, Du X, Xie G and Jiang Y 2015 Enhanced formaldehyde-sensing performances of mixed polyethyleneimine-multiwalled carbon nanotubes composite films on quartz crystal microbalance *IEEE Sens. J.* **15** 6904–11

[35] Rianjanu A, Julian T, Hidayat S N, Yulianto N, Majid N, Syamsu I, Wasisto H S and Triyana K 2020 Quartz crystal microbalance humidity sensors integrated with hydrophilic polyethyleneimine-grafted polyacrylonitrile nanofibers *Sens. Actuators* B **319** 128286

[36] Jiwei Z, Liangying Z and Xi Y 2000 The dielectric properties and optical propagation loss of *c*-axis oriented ZnO thin films deposited by sol–gel process *Ceram. Int.* **26** 883–5

[37] Pehlivan İ B, Marsal R, Georén P, Granqvist C G and Niklasson G A 2010 Ionic relaxation in polyethyleneimine-lithium bis (trifluoromethylsulfonyl) imide polymer electrolytes *J. Appl. Phys.* **108** 074102

[38] Duan Z, Jiang Y and Tai H 2021 Recent advances in humidity sensor for human body related humidity detections *J. Mater. Chem.* C **9** 14963–80
[39] Awais M, Khan M U, Hassan A, Bae J and Chattha T E 2020 Printable highly stable and superfast humidity sensor based on two dimensional molybdenum diselenide *Sci. Rep.* **10** 1–13
[40] Dwiputra M A, Fadhila F, Imawan C and Fauzia V 2020 The enhanced performance of capacitive-type humidity sensors based on ZnO nanorods/$WS_2$ nanosheets heterostructure *Sens. Actuators* B **310** 127810
[41] Fatima N, Aziz F, Ahmad Z, Najeeb M, Azmeer M, Karimov K S, Ahmed M, Basheer S, Shakoor R and Sulaiman K 2017 Compositional engineering of the pi-conjugated small molecular VOPcPhO: $Alq_3$ complex to boost humidity sensing *RSC Adv.* **7** 19780–6
[42] Hassan G, Sajid M and Choi C 2019 Highly sensitive and full range detectable humidity sensor using PEDOT: PSS, methyl red and graphene oxide materials *Sci. Rep.* **9** 1–10
[43] McGhee J R, Sagu J S, Southee D J, Evans P S and Wijayantha K U 2020 Printed, fully metal oxide, capacitive humidity sensors using conductive indium tin oxide inks *ACS Appl. Electron. Mater.* **2** 3593–600
[44] Ali S, Jameel M A, Harrison C J, Gupta A, Evans R A, Shafiei M and Langford S J 2021 Enhanced capacitive humidity sensing performance at room temperature via hydrogen bonding of cyanopyridone-based oligothiophene donor *Chemosensors* **9** 320
[45] Wahab R, Ansari S, Kim Y, Seo H, Kim G, Khang G and Shin H-S 2007 Low temperature solution synthesis and characterization of ZnO nano-flowers *Mater. Res. Bull.* **42** 1640–8
[46] Hower P and Gupta T 1979 A barrier model for ZnO varistors *J. Appl. Phys.* **50** 4847–55
[47] Wang F, Liu P, Nie T, Wei H and Cui Z 2012 Characterization of a polyamine microsphere and its adsorption for protein *Int. J. Mol. Sci.* **14** 17–29
[48] Yang B, Huang W, Li C and Li L 2006 Effects of moisture on the thermomechanical properties of a polyurethane shape memory polymer *Polymer* **47** 1348–56
[49] Jeong H, Noh Y and Lee D 2019 Highly stable and sensitive resistive flexible humidity sensors by means of roll-to-roll printed electrodes and flower-like $TiO_2$ nanostructures *Ceram. Int.* **45** 985–92
[50] Haq Y-U, Ullah R, Mazhar S, Khattak R, Qarni A A, Haq Z-U and Amin S 2022 Synthesis and characterization of 2D MXene: device fabrication for humidity sensing *J. Sci.-Adv. Mater. Dev.* **7** 100390
[51] Samaeifar F, Afifi A and Abdollahi H 2019 Implementation of PVA-nanofibers heat absorption monitoring sensor for ultrasensitive detection of 2, 4-dinitrotoluene *IEEE Sens. J.* **19** 9634–40
[52] Sajid M, Aziz S, Kim G B, Kim S W, Jo J and Choi K H 2016 Bio-compatible organic humidity sensor transferred to arbitrary surfaces fabricated using single-cell-thick onion membrane as both the substrate and sensing layer *Sci. Rep.* **6** 1–10
[53] Khan M U, Hassan G and Bae J 2019 Bio-compatible organic humidity sensor based on natural inner egg shell membrane with multilayer crosslinked fiber structure *Sci. Rep.* **9** 1–13
[54] Yang H, Ye Q, Zeng R, Zhang J, Yue L, Xu M, Qiu Z-J and Wu D 2017 Stable and fast-response capacitive humidity sensors based on a ZnO nanopowder/PVP-RGO multilayer *Sensors* **17** 2415
[55] Turkani V S, Maddipatla D, Narakathu B B, Saeed T S, Obare S O, Bazuin B J and Atashbar M Z 2019 A highly sensitive printed humidity sensor based on a functionalized MWCNT/HEC composite for flexible electronics application *Nanoscale Adv.* **1** 2311–22
[56] Gaspar C, Olkkonen J, Passoja S and Smolander M 2017 Paper as active layer in inkjet-printed capacitive humidity sensors *Sensors* **17** 1464
[57] He P, Brent J, Ding H, Yang J, Lewis D, O'Brien P and Derby B 2018 Fully printed high performance humidity sensors based on two-dimensional materials *Nanoscale* **10** 5599–606
[58] Ali S, Hassan A, Hassan G, Bae J and Lee C H 2017 All-printed humidity sensor based on graphene/methyl-red composite with high sensitivity (vol 105, pg 23, 2016) *Carbon* **112** 130